SPEKTRA: Jurnal Fisika dan Aplikasinya
Volume 11, Issue 1, April 2026
Homepage: doi.org/10.21009/SPEKTRA

DOI: doi.org/10.21009/SPEKTRA.111.05

Integrating Time-Dependent and Time-Independent Earthquake Recurrence Models for Fault-Based Seismic Hazard Assessment in the Lampung Region, Southern Sumatra

Rizki Wulandari[1,2,*], Yudha Styawan[1,2], Satria Bagus Prabowo[1]

[1]*Department of Geophysical Engineering, Institut Teknologi Sumatera, Lampung, Indonesia*
[2]*The Earthquake and Tsunami Disaster Mitigation Center, Institut Teknologi Sumatera, Lampung, Indonesia*

*Corresponding Author Email: rizki.wulandari@tg.itera.ac.id

Received: 7 December 2025
Revised: 24 April 2026
Accepted: 30 April 2026
Online: 30 April 2026
Published: 30 April 2026

SPEKTRA: Jurnal Fisika dan Aplikasinya
p-ISSN: 2541-3384
e-ISSN: 2541-3392

ABSTRACT

The Lampung region in southern Sumatra is exposed to significant seismic hazard due to its proximity to the Sunda megathrust and multiple active crustal faults. This study integrates time-independent (Poissonian) and time-dependent (Brownian Passage Time/BPT) earthquake recurrence models to evaluate fault-specific rupture probabilities and their implications for probabilistic seismic hazard assessment (PSHA). This approach systematically bridges the gap between traditional stationary models and the physical reality of seismic cycles, ensuring that the resulting hazard estimates reflect the current elapsed time since the last major rupture. Earthquake catalogs from USGS, BMKG, and historical sources were compiled for shallow events (≤50 km) between 1900–2023, and fault parameters were derived from national hazard maps and published geological studies. Recurrence intervals were estimated for 28 major fault segments across Sumatra, the Sunda Strait, and western Java. Results show strong temporal variability in seismic potential, with the Kumering South segment exhibiting the highest 50-year rupture probability (>50%) due to its elapsed time nearing the estimated recurrence interval. In contrast, segments such as Semangko West-A show markedly reduced short-term probability under the BPT model. PSHA simulations using OpenQuake reveal peak ground acceleration (PGA) values of 0.6–1.5 g for 2% exceedance in 50 years, indicating very high hazard levels in areas adjacent to the Sumatra Fault System. Incorporating time-dependent recurrence provides a more cycle-consistent spatial pattern compared to Poissonian results, reducing overestimation in early-cycle segments and enhancing hazard representation in late-cycle faults. While this study is constrained by

uncertainties in historical recurrence intervals and fault slip-rates, these findings provide a more refined academic contribution to regional hazard characterization, supporting more robust risk mitigation strategies in Lampung Province.

Keywords: seismic hazard, brownian passage time, poissonian model, recurrence interval, Lampung, Sumatra Fault System, PSHA, OpenQuake

INTRODUCTION

Indonesia is one of the most earthquake-prone countries in the world due to its position at the convergence of three major tectonic plates: the Indo-Australian Plate, the Eurasian Plate, and the Pacific Plate [1]. The interaction of these plates generates extensive subduction zones and active fault systems across the archipelago, including the western part of Java and the Sunda Strait. Among the provinces exposed to significant seismic hazards is Lampung, given its proximity to the megathrust subduction zone and the presence of several surrounding active faults [2]. Previous studies indicate that Lampung is highly vulnerable to large earthquakes originating from the subduction zone off western Sumatra, local fault systems, and active structures extending from western Java into the Sunda Strait [3].

In addition to subduction-related sources, Lampung is also influenced by active fault systems that extend both onshore and offshore. Several major fault segments have been identified in and around the province, including the Semangko Barat A, Semangko Barat B, Semangko Timur A, Semangko Timur B, Ranau, and Kumering South faults (shows in FIGURE 1). These fault zones contribute significantly to the regional seismicity and play a crucial role in accommodating crustal deformation along the southern part of Sumatra. Their activity has been associated with both moderate and large earthquakes that may affect densely populated and industrial areas of Lampung.

Based on the United States Geological Survey (USGS) earthquake catalog, several significant earthquakes have occurred in the Lampung region since 1900 [4]. The largest recorded event was a magnitude 7.5 earthquake in June 1933 with a focal depth of approximately 20 km. Other notable events include a magnitude 6.4 earthquake on April 2, 1919, with a depth of 20 km, and a magnitude 6.9 earthquake on February 15, 1994, with a depth of 23.1 km. The spatial distribution of these historical events is illustrated in FIGURE 1, showing their proximity to the identified active fault zones. These records demonstrate that Lampung has experienced repeated large-magnitude earthquakes over the past century, reflecting persistent tectonic activity and the potential for future damaging events in the region.

The occurrence of these earthquakes can be explained by the Elastic Rebound Theory, which describes how stress gradually accumulates along fault planes as tectonic plates move relative to one another [5]. When the accumulated stress exceeds the fault's frictional resistance, a sudden rupture occurs, releasing elastic energy as an earthquake. Following the rupture, the fault returns to a relatively undeformed state, initiating a new cycle of stress accumulation.

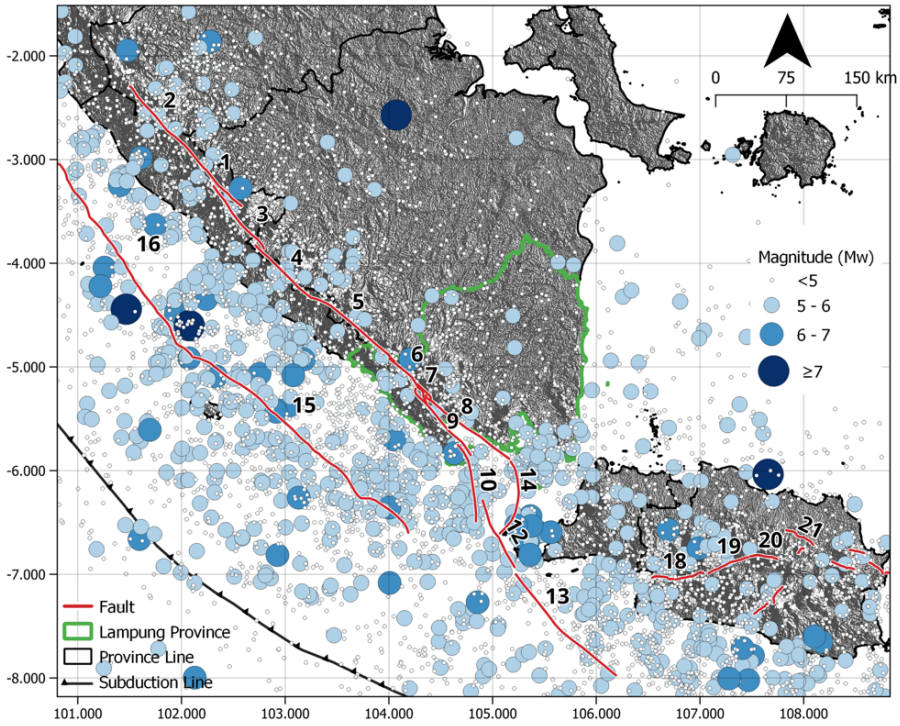

FIGURE 1. Distribution of earthquake epicenters (magnitude Mw <5 to ≥7) in western Java, the Sunda Strait, and southern Sumatra, including the Lampung Province (outlined in green). Fault traces are shown in red, the subduction zone is marked by the black line, and provincial boundaries are outlined in gray. The plotted events represent shallow earthquakes with depths up to 50 km, highlighting the seismic activity associated with both the megathrust and active crustal faults in the region.

This repetitive process forms the foundation for understanding earthquake recurrence intervals, which represent the average time between major ruptures on a given fault.

Understanding the recurrence interval is essential for probabilistic seismic hazard analysis (PSHA), as it provides insight into the temporal probability of future earthquakes. To quantify this, two probabilistic models are commonly employed: the Poisson distribution [6] and the Brownian Passage Time (BPT) model [7]. The Poisson model assumes that earthquake occurrences are random and independent over time, making it suitable for regions or faults without sufficient historical or paleoseismic data. In contrast, the BPT model is time-dependent and derived from the Elastic Rebound Theory; it considers the mean recurrence interval and the variability in stress accumulation to estimate the conditional probability of earthquake occurrence.

Building upon these models, numerous studies have applied earthquake recurrence frameworks to assess temporal earthquake probabilities in various tectonically active regions worldwide, including California, New Zealand, Japan, Turkey and Taiwan [8,9]. Similar approaches have also been adopted in other seismically active areas such as India and the Mediterranean [10-12]. These studies have been instrumental in supporting governmental efforts in land-use planning, building-code revisions, disaster preparedness, and emergency response. Owing to its capability to model stochastic stress accumulation and quantify

uncertainty in recurrence intervals, the Brownian Passage Time (BPT) model has become a primary framework for long-term, time-dependent seismic hazard assessment [3, 11, 13, 14]. It has notably formed the basis for modern forecasts such as the Uniform California Earthquake Rupture Forecast (UCERF), whose synthetic catalogs and temporal predictions have been rigorously evaluated against recent major seismic sequences [13, 14]. Despite these global advancements, a significant research gap remains in the localized application of such time-dependent frameworks within the Sumatra Fault System, particularly for the Lampung segment. Most existing seismic hazard assessments for southern Sumatra continue to rely on time-independent Poissonian assumptions, which assume earthquake occurrences are stationary. This often leads to a "memoryless" representation of risk that may either overestimate the hazard for faults early in their seismic cycle or underestimate it for those nearing the end of their recurrence interval. The state-of-the-art contribution of this study lies in bridging the gap between general tectonic theory and site-specific disaster mitigation. We address this by providing the first integrated Poisson-BPT assessment specifically tailored to the unique fault geometries of Lampung, utilizing an updated 1900–2023 catalog and national hazard parameters to move beyond static, time-independent representations.

In this study, we analyze seismicity within a 320 km radius [15] from the Lampung region, encompassing both onshore and offshore sources, including the subduction interface and surrounding active faults. We quantify the Brownian Passage Time (BPT) model for faults that possess historical earthquake records, while the Poissonian distribution is applied to faults lacking such data. This combined approach enables a more comprehensive understanding of the temporal characteristics of earthquake recurrence, improving the reliability of seismic hazard assessment in southern Sumatra, particularly in the Lampung region.

In addition to its geological vulnerability, Lampung holds a strategic economic role as a trade and industrial gateway linking Java and Sumatra [16]. The province functions as a vital transportation corridor through the Sunda Strait, serving as a hub for logistics, energy distribution, and industrial activities that connect the two most populous and economically dynamic islands of Indonesia. Thus, the potential impact of major earthquakes in this region extends beyond direct physical damage, posing significant risks to national economic stability and inter-island connectivity.

METHODS

Data Collection

Earthquake data were compiled from the United States Geological Survey (USGS) and the Indonesian Meteorological, Climatological, and Geophysical Agency (BMKG) catalogs, covering the period from 1900 to 2023. Only shallow earthquakes with focal depths ≤50 km were included, as these events are most relevant for assessing ground shaking and fault-related seismic hazard in the study region. Historical earthquake information was further integrated from multiple sources, including Gempa Nusantara [17], Sieh and Natawidjaja [2], and additional references contained in the USGS database [4]. These data were harmonized with

TABLE 1. Fault parameters used in the seismic source modeling for this study, including segment name, fault type, dip angle, maximum magnitude, slip rate, and historical earthquake information. Elapsed time since the most recent event is calculated relative to the year 2025. Data were compiled from USGS [4], BMKG [19], PuSGeN [1], and Gempa Nusantara [17].

ID	Name	Segment	Type	Dip (deg.)	Max. mag.	*Sliprate* (mm/yr)	Historical EQ.		Source of info.	Elapse time since 2025
							Last EQ.	Date		
1	Sumatran Fault	Ketaun	SS	90	7.4	13	6.8 M	15/03/1952	USGS	73
2	Sumatran Fault	Dikit	SS	90	7.2	13	6.6 Mwc	10/1/2009	USGS	16
3	Sumatran Fault	Musi	SS	90	7.3	12	6	15/12/1979	USGS	46
4	Sumatran Fault	Manna	SS	90	7.4	12	-	1893	PuSGeN 2017, Gempa Nusantara	132
5	Sumatran Fault	Ranau	SS	90	7.5	11	7.5 M	25/06/1933	USGS	92
6	Sumatran Fault	Kumering North	SS	90	7.5	12.5	7.5 M	25/06/1933	USGS	92
7	Sumatran Fault	Kumering South	SS	90	7.2	11	7.5 M	25/06/1933	USGS	92
8	Sumatran Fault	Semangko barat-A	SS	90	7.4	8	6.35 Mwc	12/4/1919	Gempa Nusantara	6
9	Sumatran Fault	Semangko Timur-A	SS	90	7.4	8	-	1908	PuSGeN 2017	117
10	Sumatran Fault	Semangko barat-B	SS	90	7.3	8	-	1908	PuSGeN 2017	117
11	Sumatran Fault	Semangko Timur-B	SS	90	6.9	3	6.05 Mw	26/04/1964	Gempa Nusantara	61
12	Sumatran Fault	Ujung Kulon A	SS	90	7.4	10	5.1 Mb	11/4/2015	Gempa Nusantara	10
13	Sumatran Fault	Ujung Kulon B	SS	90	7.6	10	5.1 Mb	10/11/2021	Gempa Nusantara	4
14	Sumatran Fault	Semangko Graben	N	90	7.1	3	7.5	17/3/1905	USGS	120
15	Mentawai Fault	Enggano	RW	45	7.7	5	7.9	4/6/2000	USGS	25
16	Mentawai Fault	Mentawai	RW	45	8.5	5	6.9 Mwb	16/01/2001	USGS	24
17	Cimandiri	Cimandiri	RS	45	6.7	2	5.6	21/10/2022	USGS	1
18	Cimandiri	Nyalidung Cibeber	RS	45	6.9	0.5	4.7	30/10/2006	USGS	14
19	Cimandiri	Rajamandala	SS	90	7	0.1	4.4	15/04/2002	USGS	3
20	Lembang	Lembang	SS	90	7	4.5	3.3	28/08/2011	BMKG	19
21	Baribis Kendeng Fault	Subang	RS	45	6.9	0.5	5.1 M	10/3/2020	BMKG	23
22	Baribis Kendeng Fault	Cirebon-1	RS	45	6.5	0.5	-	-		-
23	Baribis Kendeng Fault	Cirebon-2	RS	45	6.5	0.1	-	-		-
24	Baribis Kendeng Fault	Brebes	RS	45	6.5	0.1	-	-		-
25	Baribis Kendeng Fault	Tampomas	RS	60	6.5	0.5	-	-		-
26	Garsela Fault	Rakutai	N	60	6.5	0.1	4.5 Mb	2/1/2023	USGS	5
27	Garsela Fault	Kencana	SS	90	6.5	0.1	4.5 MB	2/1/2023	USGS	2
28	Ciremai	Ciremai	SS	90	6.6	0.5	4.4 Mb	25/07/2024	USGS	2

the empirical magnitude conversion relationships adopted by PuSGeN [1], allowing consistency across different historical and instrumental catalogs.

Fault traces were obtained primarily from the 2017 Indonesian Earthquake Source and Hazard Map [1], supplemented with updated active fault databases and published geological studies. In defining fault segmentation, a maximum fault length of approximately 320 km was applied, following international guidelines for seismic source modeling [18]. This provides a standardized basis for recurrence interval estimation and ensures comparability with global practices in fault-based seismic hazard assessment. For this study, the main fault system of interest extends approximately 320 km across the Sunda Strait and western Java region, comprising both onshore and offshore segments that are seismically active and pose direct implications for Lampung Province shows in TABLE 1. Active fault systems were identified and segmented based on geological and seismotectonic studies. For each fault segment, key parameters such as length, slip rate, and characteristic earthquake magnitude were compiled from published sources and, where necessary, estimated using empirical relationships. Based on these data, faults were classified into two groups: those with sufficient historical records for time-dependent (BPT) analysis and those with limited data assigned to the time-independent (Poissonian) model.

Recurrence Interval Estimation

Statistical models for earthquake recurrence have been formulated based on empirical analyses of earthquake recurrence intervals [15, 20, 21]. This study adopts a quantitative approach by integrating statistical and physics-based models to estimate earthquake recurrence intervals along active fault systems. Two probabilistic models are utilized: the Poissonian model [6] and the Brownian Passage Time (BPT) model [7]. The analysis incorporates geological parameters—including fault length, slip rate, and characteristic displacement—along with seismic catalogs and historical earthquake records. Because historical earthquake data are limited for several fault segments, the Poissonian distribution is employed to account for the recurrence interval under data constraints. In addition, this study aims to compare the performance and implications of the Poissonian and BPT models in representing earthquake recurrence behavior. The resulting recurrence estimates are subsequently integrated into a probabilistic seismic hazard assessment (PSHA) framework to evaluate their implications for seismic hazard in Lampung Province.

The Poissonian model is the conventional method for earthquake recurrence, assuming that earthquake occurrence is a memoryless process—events occur randomly in time, independent of when the last earthquake occurred [6, 22]. The probability that no earthquake occurs during a time interval t is given by:

$$P(t) = e^{-\lambda t}, \quad (1)$$

where $\lambda = \frac{1}{\mu}$ is the average rate of earthquake occurrence, μ is the mean recurrence interval, and t is the elapsed time since the last event.

This model is simple and widely used but does not account for the physical stress-accumulation process along active faults. As such, it tends to underestimate or overestimate hazard depending on where the system lies within the earthquake cycle.

To address the limitations of the Poissonian approach, this study applies the Brownian Passage Time (BPT) model, which combines renewal theory with a stochastic framework. The BPT model considers earthquake occurrence as a stress-renewal process, where the next earthquake happens once accumulated tectonic stress reaches a threshold. This process is modeled as the first-passage time of a Brownian particle with drift. The probability density function of the BPT model is given by [7]:

$$f(t) = \frac{1}{\sqrt{2\pi\alpha t}} \exp\left(-\frac{(t-\mu)^2}{2(\alpha\mu)^2 t}\right), \quad (2)$$

where t time since the last earthquake (years), μ is mean recurrence interval, and α is coefficient of variation (standard deviation divided by mean), representing irregularity in the cycle. In this assessment, the BPT parameter α was assigned a value of 0.5 to represent the typical aperiodicity of fault ruptures.

The BPT model allows for variability in recurrence times, producing a probability distribution rather than a fixed mean. This makes it more realistic in capturing the uncertainty of earthquake cycles. Both Poissonian and BPT recurrence intervals were calculated for the identified fault segments in the Sunda Strait and western Java. The Poissonian results provide a baseline, while the BPT outputs allow for a time-dependent hazard characterization. The estimated recurrence distributions are then integrated into PSHA to calculate the annual rate of exceedance for ground motion intensities relevant to Lampung.

The Probabilistic Seismic Hazard Assessment (PSHA) approach was applied to quantify the likelihood of different levels of ground shaking at a site or region over a specified time period. Unlike deterministic methods, PSHA incorporates the uncertainties associated with earthquake source locations, magnitudes, recurrence intervals, and ground-motion attenuation, thereby providing a comprehensive estimation of seismic hazard. The method follows the classical formulation established by Cornell [6], which integrates the contributions of all potential seismic sources within the study area expressed as:

$$\lambda(\mathrm{IM} > \mathrm{x}) = \sum_{i=1}^{n_{\mathrm{source}}} \lambda(\mathrm{M_i} > \mathrm{M_{min}}) \int_{\mathrm{M_{min}}}^{\mathrm{M_{max}}} \int_{0}^{\mathrm{r_{max}}} \mathrm{P}(\mathrm{IM} > \mathrm{x}\,|\mathrm{m,r}) \mathrm{f_{m_i}}(\mathrm{m}) \mathrm{f_{Ri}}(\mathrm{r})\, \mathrm{dr}\, \mathrm{dm}. \quad (3)$$

Here, λ denotes the rate at which a ground-motion intensity measure (IM) exceeds a threshold value x. The summation over $i = 1{:}n$ accounts for the contributions of all seismogenic sources, incorporating the magnitude-dependent occurrence rates λ associated with each source. The term $\mathrm{P}(\mathrm{IM} > \mathrm{x}\,|\mathrm{m,r})\mathrm{f_{m_i}}(\mathrm{m})\mathrm{f_{Ri}}(\mathrm{r})$ reflects the inclusion of earthquake ruptures across the full range of magnitudes and source-to-site distances. For every possible rupture scenario, the probability that ground-motion level x will be exceeded at the site is evaluated.

In this research, we focus exclusively on modeling the activity of fault sources using both time-dependent and time-independent approaches to gain deeper insights into their behavior.

All PSHA calculations were performed using the OpenQuake engine developed by the Global Earthquake Model (GEM) Foundation—an open-source platform for seismic hazard and risk assessment [23].

RESULTS AND DISCUSSION

FIGURE 2 presents the 50-year earthquake occurrence probabilities for major fault segments influencing Lampung Province, derived from the combined Poissonian and Brownian Passage Time (BPT) recurrence models. These results reflect the time-independent (segment IDs: 1,2,3,4,5,6,7,8,9,10,11,12,13,14,15,16, and 20) and time-dependent behavior of segment (segment IDs: 17,18,19,21,22,23,24,25,26,27, and 28), respectively, and highlight spatial variations in seismic potential across Sumatra, the Sunda Strait, and western Java. The map shows that several segments of the Semangko Fault system—particularly Kumering North (ID 6), Kumering South (ID 7), Semangko Barat-B (ID 9), and Semangko Timur-A (ID 10)—exhibit elevated 50-year rupture probabilities, commonly ranging from 15% to more than 40%. These segments lie closest to the Lampung mainland and have relatively well-constrained geological parameters, including moderate slip rates (TABLE 1). As a result, the BPT model

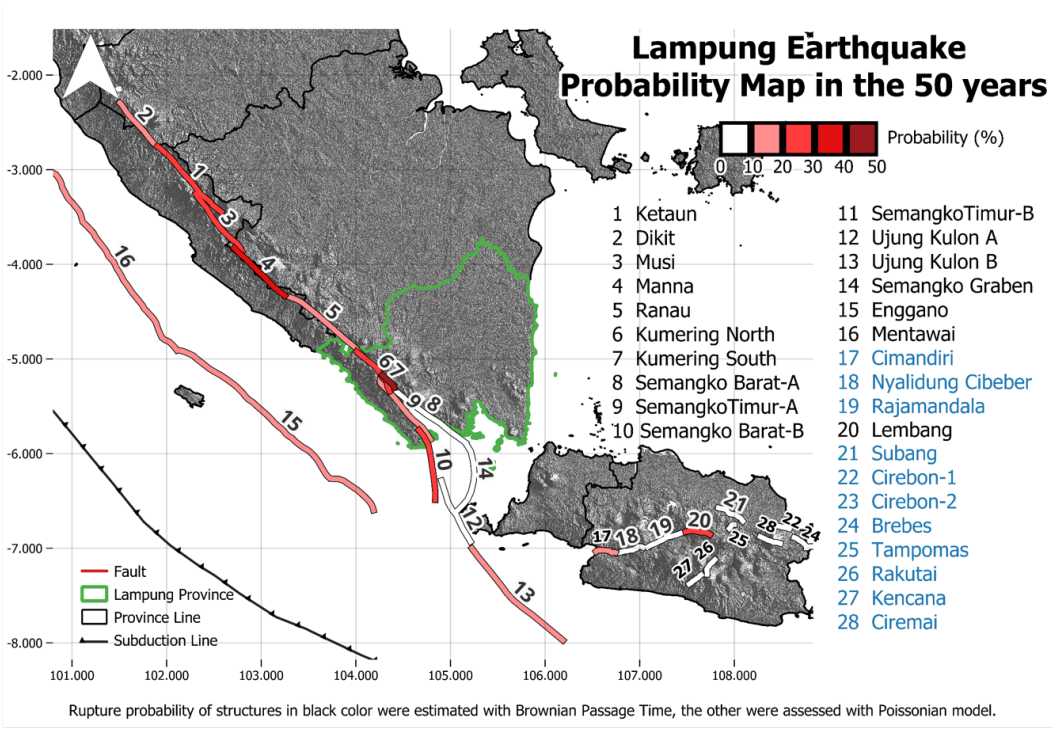

FIGURE 2. Spatial distribution of 50-year earthquake rupture probabilities for major active faults affecting Lampung Province. Fault segments are symbolized according to their rupture probability classes, ranging from <10% to >50%, and are labeled with their corresponding numerical IDs (1–28). Black-highlighted segments indicate faults analyzed with the Brownian Passage Time (BPT) model due to available historical recurrence constraints, whereas the remaining segments were assessed using the Poissonian recurrence model. The map also shows the Lampung provincial boundary (green), regional fault traces (red), and the Sunda subduction interface (black).

indicates that these faults are progressing toward later stages of their earthquake cycles, producing higher time-dependent probabilities than the Poisson model alone would suggest.

In contrast, fault segments farther from Lampung, such as Ketaun, Dikit, and Musi in the northern part of the Sumatran fault system, display comparatively reduced probabilities (typically <10–20%). These faults have longer recurrence intervals and less frequent historical seismicity, leading to lower Poissonian rates and broad uncertainty ranges in the BPT distributions.

The western Java faults—including Cimandiri, Lembang, Rajamandala, Subang, and Cirebon—show moderate rupture probabilities, mostly between 10% and 30%. Although these segments are located outside Lampung Province, their inclusion is important because large events in western Java have the potential to generate long-period ground motions that can propagate across the Sunda Strait. Segments such as Lembang and Cimandiri show slightly higher probabilities relative to adjacent structures, consistent with their documented activity in recent centuries and relatively shorter recurrence intervals reported in previous geological studies.

As indicated in the map annotation, fault segments shown in black were modeled using the Brownian Passage Time (BPT) method due to the availability of historical rupture data. These faults typically show stronger sensitivity to elapsed time since the last event. In several cases, the BPT model yields higher rupture probabilities than the Poissonian model because it accounts for accumulated tectonic stress and cycle irregularity.

The seismic hazard map for Lampung Province is presented in FIGURE 3, illustrating the peak ground acceleration (PGA) values corresponding to a 2% probability of exceedance within 50 years. This calculation is based on earthquake occurrence rates derived from the time-independent Poissonian model. PGA values with 2% and 10% exceedance probabilities over 50 years are commonly applied as reference levels in standard engineering design. However, these thresholds are not absolute scientific justifications and are still considered ambiguous; consequently, research continues to advance toward more risk-informed approaches [15, 24, 25]. In Indonesia, the 10% PGA value has remained the minimum design standard for building construction, as regulated in SNI-03-1726-2002 and subsequently revised through the latest SNI-1726-2019, which continues to account for bedrock ground-motion parameters [26].

The resulting map indicates a gradual increase in PGA from the northeast toward the southwest, with the highest values occurring near the active segments of the Sumatra Fault System. The highest accelerations are identified around the Kumering North (ID 6), Kumering South (ID 7), Semangko West-A (ID 8), and Semangko West-B (ID 9) segments. In areas directly adjacent to these segments, PGA values range from 0.6 to 1.5 g, significantly exceeding the threshold for high seismic hazard classification established in the Badan Nasional Penanggulangan Bencana No. 02/2012, which defines high hazard as PGA > 0.7 g [27]. Thus, PGA values around these fault segments can be categorized as very high, exceeding more than twice the lower bound of the high-hazard class.

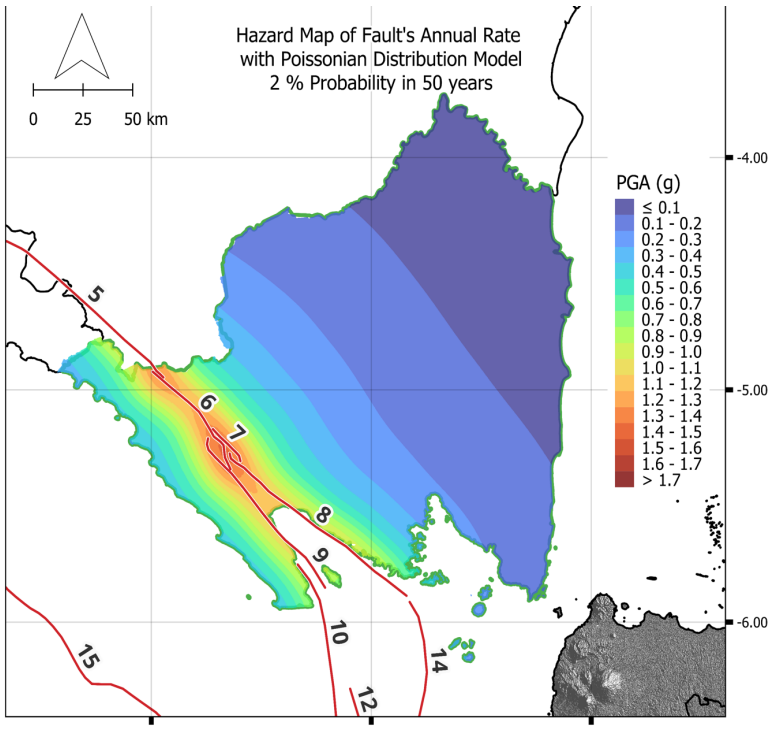

FIGURE 3. Hazard map illustrating peak ground acceleration (PGA) corresponding to a 2% probability of exceedance in 50 years for Lampung Province, based on the annual occurrence rates derived from the Poissonian (time-independent) model. The map displays spatial variations in ground shaking intensity, with elevated PGA levels. Fault traces are shown in red, and the provincial boundary is outlined in green.

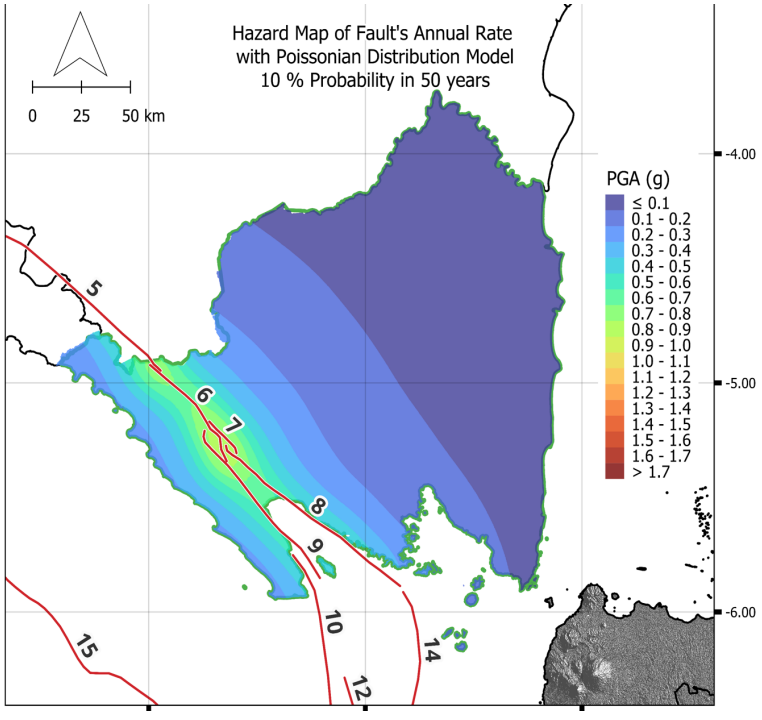

FIGURE 4. Hazard map illustrating peak ground acceleration (PGA) corresponding to a 10% probability of exceedance in 50 years for Lampung Province, based on the annual occurrence rates derived from the Poissonian (time-independent) model. The map displays spatial variations in ground shaking intensity, with elevated PGA levels. Fault traces are shown in red, and the provincial boundary is outlined in green.levels. Fault traces are shown in red, and the provincial boundary is outlined in green.

The Poissonian approach used in this computation assumes that earthquake occurrence follows a random, memoryless process, meaning that the average occurrence rate becomes the main driver in seismic hazard estimation [13, 14]. Consequently, the active segments of the Sumatra Fault System particularly Kumering North (ID 6), Kumering South (ID 7), Semangko West-A (ID 8), and Semangko West-B (ID 9) produce high PGA values due to their slip rates of 8–12.5 mm/year and maximum magnitude potential of Mw 7.2–7.5. Geological observations further indicate that the southern part of the fault may generate recurring earthquakes of Mw 7.2–7.4 approximately every ~100 years [2] . This finding aligns with the average slip rate of ~11 mm/year (ranging from 5–27 mm/year), estimated from cumulative seismic moment release along each segment and magnitude estimations for 100- and 200-year recurrence intervals [2]. In addition, the Indonesian Seismic Hazard Map identifies Lampung as one of the regions with the highest PGA levels in southern Sumatra due to its close proximity to active fault segments [31].

Beyond shallow crustal sources, the subduction zone between the Indo-Australian and Eurasian plates southwest of Lampung contributes significantly to elevated PGA values, particularly along the coastal regions of West Lampung and South Pesisir [22, 28]. Studies by Widiyantoro et al. [29] and Supendi et al. [30] have identified a seismic gap beneath southern Java and Sumatra, interpreted as a region of accumulated tectonic stress with the potential to generate a megathrust earthquake. Such large megathrust events are capable of producing long-period ground motions that propagate efficiently across the Sunda Strait toward the eastern regions. Therefore, the combination of shallow crustal fault sources and the Sunda subduction zone places Lampung among the areas with the highest seismic hazard levels in southern Sumatra.

The primary difference between PGA values with 10% and 2% probabilities of exceedance within 50 years lies in their corresponding return periods. A PGA with a 10% probability of exceedance in 50 years, equivalent to a return period of approximately 475 years, is commonly used as the design standard for general infrastructure in many modern building codes, including SNI 1726-2019 [26]. Conversely, a PGA with a 2% probability of exceedance in 50 years (corresponding to a return period of about 2475 years) represents rare but potentially highly destructive earthquake scenarios. This standard refers to the International Building Code (IBC) 2009, which specifies a 2% exceedance probability within 50 years as the design basis for large-magnitude, long-return-period earthquakes. The provision was later adopted into SNI 1726:2012 on “Seismic Design Requirements for Buildings and Non-Building Structures” [31].

Although the spatial distribution patterns of the two hazard maps (10% and 2%) appear relatively similar both showing an increase in seismic intensity from the northeast toward the southwest following the proximity to the Sumatra Fault System and the subduction interface between the Indo-Australian and Eurasian plates the PGA values in the 2% exceedance map are noticeably higher than those in the 10% map. This difference can be observed by comparing FIGURE 3 (2% probability) and FIGURE 4 (10% probability), particularly in areas adjacent to the active fault segments such as Kumering North (ID 6), Kumering South (ID 7), Semangko West-A (ID 8), and Semangko West-B (ID 9). In the 2% exceedance map, these

regions are represented by darker color shades (ranging from 0.6–1.5 g), whereas in the 10% map, they appear lighter (ranging from 0.4–1.0 g).

The time-dependent seismic hazard map (BPT model) for Lampung Province with a 2% probability of exceedance in 50 years is presented in FIGURE 5, explicitly incorporating the position of each fault segment within its stress-accumulation cycle. Unlike the Poissonian hazard map at the same exceedance level (FIGURE 3), the BPT map displays sharper localized variations in ground-shaking intensity, particularly along segments that are approaching the end of their seismic cycle. This pattern arises because the BPT model amplifies the contribution of segments with long elapsed times and ratios that approach or exceed their mean recurrence intervals, thereby increasing the estimated hazard not only as a function of slip rate and maximum magnitude but also as a consequence of the time proximity to the next potential rupture [13, 14].

The most prominent increase in seismic hazard is observed on the Kumering South Segment (ID 7). As shown in TABLE 2, this segment exhibits a substantially elevated annual occurrence rate under the BPT model (0.0100), compared to its Poissonian rate (0.0076). This elevated probability results from the elapsed time on the Kumering South Segment, which has reached 92 years since the last major earthquake in 1933. This duration nearly matches its estimated mean recurrence interval of approximately 99 years. Visually, this condition is represented by a broad zone of high-intensity PGA contours (1.3–1.4 g) surrounding this segment in FIGURE 5, indicating that the segment is in a late-cycle state and producing the highest 50-year probability of rupture in the study area (50.22%).

In contrast, a notable reduction in hazard levels is observed for the Semangko West-A Segment (ID 8). The BPT model yields an annual occurrence rate that drops drastically to 8.00×10^{-6} compared to its Poissonian value of 0.0036, indicating that within the BPT framework, this segment remains in the early phase of its stress-accumulation cycle. Consequently, its contribution to hazard in FIGURE 5 appears significantly lower than in the Poissonian map. Meanwhile, the Kumering North Segment (ID 6) and the Semangko East-A Segment (ID 9) are situated in mid-cycle conditions that do not produce substantial short-term hazard anomalies. This is reflected in their nearly identical BPT and Poissonian annual rates—0.00455 vs. 0.00464 for ID 6, and 0.00361 vs. 0.00365 for ID 9—indicating that neither segment is close to a late-cycle loading stage that would elevate rupture probability.

Nevertheless, the BPT map still displays more continuous PGA contours along adjacent segments compared to the Poissonian map, which shows patchy color variations (i.e., reductions in PGA) within the same segments. The most notable contrast appears in the cluster of four adjacent segments (ID 6, 7, 8, and 9) under extreme hazard scenarios. The Poissonian model produces the highest PGA values (1.4–1.5 g) concentrated along segments ID 6 and ID 8, as it assumes cumulative contributions from time-independent average rates. In contrast, the BPT model shows slightly lower PGA values (1.3–1.4 g) and places all four neighboring segments within the same color class. This occurs because the BPT approach emphasizes the hazard contribution from segments nearing rupture, while downweighting segments that are not yet close to their next cycle (such as ID 8). As a result, the BPT map provides a physically

TABLE 2. Estimated seismic recurrence parameters for each fault segment based on two probabilistic approaches: the Truncated Exponential model representing time-independent (Poissonian) behavior, and the Brownian Passage Time (BPT) model representing time-dependent fault loading. Annual occurrence rates, 50-year probabilities of exceedance (PoE), and recurrence intervals are shown for both models, highlighting differences in long-term versus cycle-dependent rupture potential.

ID	Truncated Exponential Model			Brownian Passage Time		
	Annual Rate	PoE in 50 years (%)	Recurrence Interval (years)	Annual Rate	PoE in 50 years (%)	Recurrence Interval (years)
1	0.005942146	25.70	168.2893557	0.006028133	30.05	165.8888487
2	0.008993803	36.22	111.1876747	0.00406224	20.27	246.1696171
3	0.006748096	28.64	148.1899508	0.005000482	24.94	199.9807381
4	0.005485058	23.99	182.3134687	0.007927338	39.48	126.1457426
5	0.004086888	18.48	244.6849822	0.003343584	16.69	299.0803085
6	0.00464419	20.72	215.3227843	0.004550337	22.7	219.763938
7	0.007610141	31.65	131.4036155	0.010094781	50.22	99.06108629
8	0.003656706	16.71	273.470203	8.00003E-06	0.04	124999.5
9	0.003656706	16.71	273.470203	0.00361051	18.02	276.9691775
10	0.004498731	20.14	222.2849263	0.005468927	27.27	182.8512128
11	0.003864749	17.57	258.7490389	0.001258792	6.29	794.4124547
12	0.004570882	20.43	218.7761624	9.80048E-05	0.49	10203.58162
13	0.003019952	14.02	331.1311215	0	0	-
14	0.002845255	13.26	351.4622988	0.001977955	9.88	505.5727097
15	0.006652272	28.30	150.3245788	0.002276589	11.37	439.2535482
16	0.005740768	24.95	174.192718	0.001186704	5.93	842.6702215
17	0.003199116	14.78	312.5863464	0	0	-
18	0.00077085	3.78	1297.268867	0.000186017	0.93	5375.844071
19	0.000104713	0.52	9549.92586	2E-06	0.01	499999.5
20	0.004712078	20.99	212.2205747	0	0	0
21	0.00077085	3.78	1297.268867	0	0	-
22	0.000829793	4.06	1205.119172	-	-	-
23	0.000165959	0.83	6025.595861	-	-	-
24	0.000165959	0.83	6025.595861	-	-	-
25	0.000829793	4.06	1205.119172	-	-	-
26	0.000226464	1.13	4415.704474	0	0	-
27	0.000295121	1.46	3388.441561	0	0	-
28	0.001199416	5.82	833.7387669	0	0	-

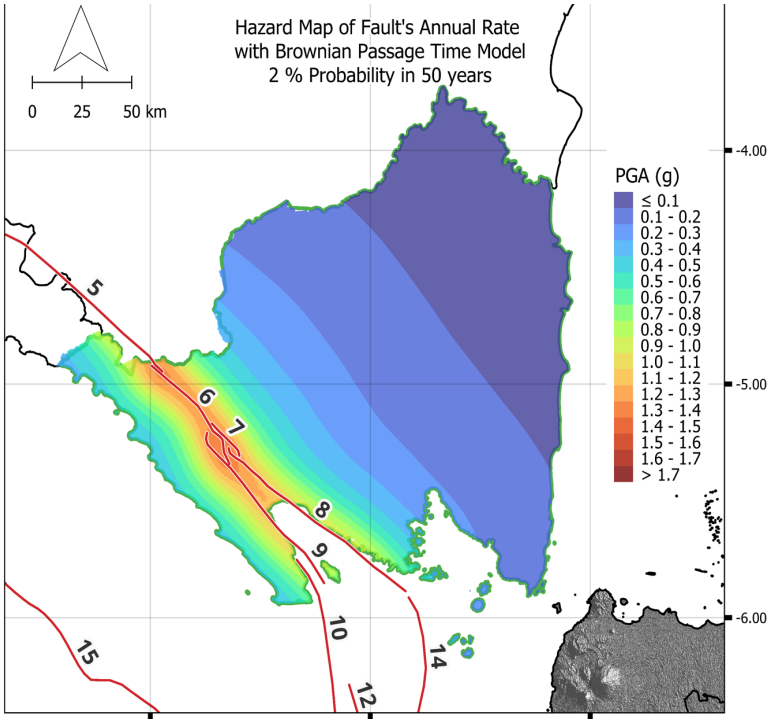

FIGURE 5. Hazard map illustrating peak ground acceleration (PGA) corresponding to a 2% probability of exceedance in 50 years for Lampung Province, based on the annual occurrence rates derived from the Brownian Passage Time Model (time-dependent) model. The map displays spatial variations in ground shaking intensity, with elevated PGA levels. Fault traces are shown in red, and the provincial boundary is outlined in green.

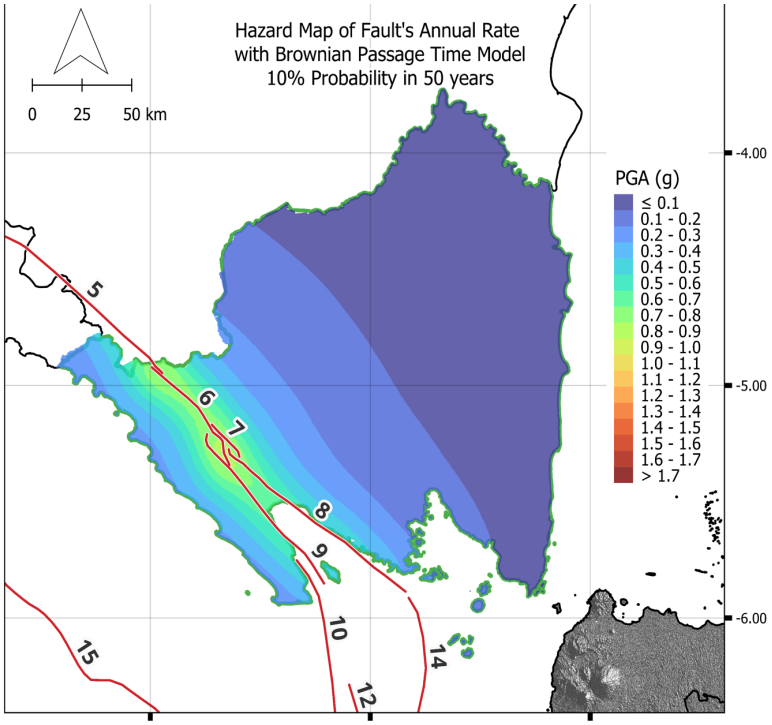

FIGURE 6. Hazard map illustrating peak ground acceleration (PGA) corresponding to a 10% probability of exceedance in 50 years for Lampung Province, based on the annual occurrence rates derived from the Brownian Passage Time Model (time-dependent) model. The map displays spatial variations in ground shaking intensity, with elevated PGA levels. Fault traces are shown in red, and the provincial boundary is outlined in green.

consistent and cycle-consistent representation of seismic hazard across closely spaced fault zones.

The Poissonian model (FIGURE 4) and the BPT model (FIGURE 6), both representing PGA values with a 10% probability of exceedance in 50 years, exhibit a similar general pattern across the four adjacent segments (Kumering North, ID 6, Kumering South, ID 7, Semangko West-A, ID 8, and Semangko West-B, ID 9). In both models, the highest PGA values are concentrated around segments ID 6 and ID 8, reaching 0.8–0.9 g. However, a notable difference appears in the distribution of the slightly lower PGA range (0.7–0.8 g). In the BPT model (FIGURE 6), the 0.7–0.8 g contours extend consistently along the trace of the Kumering North Segment (ID 6), located outside the 0.8–0.9 g closure, indicating a more uniformly distributed hazard along this segment even though it does not reach the peak PGA level.

In contrast, the Poissonian model (FIGURE 4) does not exhibit a continuous 0.7–0.8 g contour along Segment ID 6 instead, the color closure appears fragmented and re-emerges at the northwestern end of Segment ID 6 near the Ranau Segment (ID 5). This suggests that, under the Poissonian model, the 0.7–0.8 g hazard contribution from Segment ID 6 is not evenly distributed but is instead concentrated in specific localized areas. This difference in contour distribution reflects how the BPT model—by incorporating earthquake cycle information—distributes seismic hazard differently compared to the Poissonian model, which relies solely on time-independent average occurrence rates.

The highest PGA values at the 2% exceedance level in the Poissonian model are found in small portions of Segments 6 and 8 a similar pattern is also observed in the 10% exceedance maps of both the BPT and Poissonian models. This phenomenon is influenced by slip rate, maximum magnitude, and attenuation characteristics. Based on TABLE 1, the slip rate of Segment 6 (12.5 mm/yr) is the highest among Segments 7, 8, and 9, while Segment 8 exhibits a slip rate of 8 mm/yr and Segment 7 reaches 11 mm/yr. Furthermore, the maximum magnitudes of these segments are Mw 7.5 for Segment 6, Mw 7.2 for Segment 7, and Mw 7.4 for Segment 8.

Larger earthquake magnitudes generate much stronger initial seismic energy, reducing the relative effect of attenuation because high-energy seismic waves do not decay rapidly as they propagate away from the source. According to Bozorgnia et al [32], ground-motion attenuation represents the relationship between earthquake parameters—such as acceleration, velocity, displacement, intensity, and magnitude—and the distance between the source and the recording instrument, whether measured as epicentral, hypocentral, or rupture distance. While many factors influence attenuation, distance remains the primary control on ground-shaking severity at a given location. In this study, the attenuation function follows PuSGeN [1], ensuring that seismic-wave decay estimates reflect empirical characteristics of Indonesia. These conditions explain why Segments 6 and 8 exhibit higher PGA values in certain localized areas.

However, in FIGURE 5, the PGA values surrounding the cluster of four adjacent segments appear relatively uniform. This occurs because the BPT model for the 2% exceedance scenario (representing very rare earthquakes) evaluates each segment's contribution under conditions approaching its maximum possible magnitude, consistent with the 2475-year return period. As

a result, the PGA values of the four active segments become numerically similar (a hazard-saturation effect). The near-equivalence of these values produces uniform color representation due to spatial interpolation and color-class binning on the hazard map.

In addition, the elevated PGA observed in small areas on Segments 6 and 8 is also influenced by the spatial interpolation process of the hazard map. Since these two segments lie between Segments 7 and 9 which contribute high hazard levels the interpolation algorithm merges PGA values from adjacent high-hazard sources, creating a localized high-value contour zone centered in these areas. Segment 7 also exhibits substantial earthquake potential, as indicated by its highest POE value of 50.22%. Its annual BPT rate is higher than that of the Poissonian model, with a BPT recurrence interval of 99 years. By 2025, the segment has reached the 92nd year since its last major event, further supporting its elevated hazard contribution.

CONCLUSIONS

This study successfully integrated two main types of models within Probabilistic Seismic Hazard Assessment (PSHA): the time-dependent model, namely Brownian Passage Time (BPT), and the time-independent model, namely Poissonian. This model combination provides a more comprehensive depiction of the earthquake hazard from active faults in the Lampung region, Southern Sumatra. The main findings clearly highlight the critical role of the time factor. The BPT model indicates an increase in hazard for fault segments nearing their rupture time. For instance, the Kumering Selatan Segment (ID 7) exhibits the highest rupture probability over the next 50 years, exceeding 50 percent. This elevated figure is because the elapsed time since the last major earthquake (92 years) is nearly equal to its estimated mean recurrence interval (99 years). Conversely, the BPT model also shows a significant reduction in risk for segments that recently experienced an earthquake and are in their early cycle phase, such as the Semangko Barat-A Segment (ID 8).

Overall, Lampung faces an exceptionally high level of seismic hazard, with PGA values for rare earthquakes (2475-year return period) reaching between 0.6 to 1.5 g. This extreme shaking is driven by large maximum magnitudes and fast slip rates. Notably, the BPT model provides a more uniform, cycle-consistent hazard representation along active faults compared to the patchy patterns of the Poissonian map. This occurs because the BPT model evaluates each segment's contribution approaching its maximum possible earthquake strength during rare scenarios. Despite these insights, this study is limited by the uncertainties inherent in historical rupture data and the sensitivity of BPT results to the chosen aperiodicity parameters. In conclusion, integrating the BPT model yields a seismic hazard representation that is more consistent with the earthquake cycle. These findings are crucial for supporting risk mitigation efforts and revising building codes in Lampung Province to ensure infrastructure resilience against very strong ground shaking.

ACKNOWLEDGEMENTS

This work was financially supported by an internal grant from Institut Teknologi Sumatera for early-career lecturers, under contract No.1998r/IT9.2.1/PT.01.03/2025. I would like to express my sincere gratitude to the research team and all collaborators for their valuable contributions throughout the project.

REFERENCES

[1] Pusat Studi Gempa Nasional, *Peta Sumber dan Bahaya Gempa Indonesia Tahun 2017 (Map of Indonesia Earthquake Sources and Hazards in 2017)*. Bandung, Indonesia: Pusat Penelitian dan Pengembangan Perumahan Pemukiman, Kementerian PUPR, 2017.

[2] D. H. Natawidjaja and W. Triyoso, "The Sumatran fault zone — From source to hazard," *J. Earthquake Tsunami*, vol. 1, no. 1, pp. 21–47, 2007, doi: 10.1142/S1793431107000031.

[3] K. Sieh and D. Natawidjaja, "Neotectonics of the Sumatran fault, Indonesia," *J. Geophys. Res.*, vol. 105, no. B12, pp. 28295–28326, Dec. 2000, doi: 10.1029/2000JB900120.

[4] U.S. Geological Survey. (2025). ANSS Comprehensive Earthquake Catalog (ComCat) [Online]. Available: https://earthquake.usgs.gov/data/comcat/

[5] H. F. Reid, "The elastic-rebound theory of earthquakes," *Bull. Dept. Geol. Univ. Calif. Publ.*, vol. 6, no. 19, pp. 413–444, 1911.

[6] C. A. Cornell, "Engineering seismic risk analysis," *Bull. Seismological Soc. Amer.*, vol. 58, no. 5, pp. 1583–1606, Oct. 1968, doi: 10.1785/BSSA0580051583.

[7] M. V. Matthews, "A Brownian model for recurrent earthquakes," *Bull. Seismological Soc. Amer.*, vol. 92, no. 6, pp. 2233–2250, Aug. 2002, doi: 10.1785/0120010267.

[8] W. Wang and J. Hu, "Updated hazard and risk assessment for middle-southern Turkiye by PSHA methods after two damaged earthquakes in 2023," *Eng. Geol.*, vol. 358, p. 108391, Nov. 2025, doi: 10.1016/j.enggeo.2025.108391.

[9] F. Zahoor et al., "Seismic hazard assessment of Kashmir region using logic tree approach: Focus on sensitivity of PSHA results towards declustering procedures and GMPEs," *Pure Appl. Geophys.*, vol. 180, no. 3, pp. 789–827, Mar. 2023, doi: 10.1007/s00024-023-03239-5.

[10] R. B. S. Yadav et al., "An application of regional time and magnitude predictable model for long-term earthquake prediction in the vicinity of October 8, 2005 Kashmir Himalaya earthquake," *Nat. Hazards*, vol. 54, no. 3, pp. 985–1014, Sept. 2010, doi: 10.1007/s11069-010-9519-4.

[11] T. Parsons, "Recalculated probability of M ≥ 7 earthquakes beneath the Sea of Marmara, Turkey," *J. Geophys. Res.*, vol. 109, no. B5, p. 2003JB002667, May 2004, doi: 10.1029/2003JB002667.

[12] B. Pace et al., "Layered seismogenic source model and probabilistic seismic-hazard analyses in Central Italy," *Bull. Seismological Soc. Amer.*, vol. 96, no. 1, pp. 107–132, Feb. 2006, doi: 10.1785/0120040231.

[13] W. H. Savran et al., "Pseudoprospective evaluation of UCERF3-ETAS forecasts during the 2019 Ridgecrest sequence," *Bull. Seismological Soc. Amer.*, vol. 110, no. 4, pp. 1799–1817, Aug. 2020, doi: 10.1785/0120200026.

[14] M. T. Page and N. J. Van Der Elst, "Turing-style tests for UCERF3 synthetic catalogs," *Bull. Seismological Soc. Amer.*, vol. 108, no. 2, pp. 729–741, Apr. 2018, doi: 10.1785/0120170223.

[15] M. C. Gerstenberger et al., "Probabilistic seismic hazard analysis at regional and national scales: State of the art and future challenges," *Rev. Geophys.*, vol. 58, no. 4, e2019RG000653, 2020, doi: 10.1029/2019RG000653.

[16] Y. Anggraini and D. S. Kartini, "Public goods, fiscal gaps, and road decay in Lampung: A political economy perspective," *Populis*, vol. 20, no. 1, pp. 94–109, Aug. 2025, doi: 10.30598/populis.20.1.94-109.

[17] S. S. Martin et al., "Gempa Nusantara: A database of 7380 macroseismic observations for 1200 historical earthquakes in Indonesia from 1546 to 1950," *Bull. Seismological Soc. Amer.*, vol. 112, no. 6, pp. 2958–2980, Dec. 2022, doi: 10.1785/0120220047.
[18] U.S. Nuclear Regulatory Commission, "Regulatory Guide 1.208: A performance-based approach to define the site-specific earthquake ground motion," U.S. Nuclear Regulatory Commission, Washington, DC, Rep. RG 1.208, 2007.
[19] BMKG. (2025). EQ Repository | BMKG [Online]. Available: https://repogempa.bmkg.go.id/
[20] P. M. Shearer, *Introduction to Seismology*. Cambridge, U.K.: Cambridge Univ. Press, 2019.
[21] X. Guo and Z. Dai, "A method for estimating the coefficient of variation of large earthquake recurrence interval based on paleoseismic sequences," *Geosci.*, vol. 15, no. 9, p. 347, Sep. 2025, doi: 10.3390/geosciences15090347.
[22] M. A. Pangaribuan et al., "Analisis pendugaan bahaya kegempaan di batuan dasar untuk wilayah Lampung menggunakan metode PSHA," *J. Geofisika Eksplorasi*, vol. 5, no. 3, pp. 174–184, 2019, doi: 10.23960/jge.v5i3.32.
[23] M. Pagani et al., "The 2018 version of the Global Earthquake Model: Hazard component," *Earthquake Spectra*, vol. 36, no. 1S, pp. 226–251, Oct. 2020, doi: 10.1177/8755293020931866.
[24] M. C. Gerstenberger et al., "Is our true understanding of earthquake occurrence reflected in modern building codes?," in *Proc. 16th World Conf. Earthquake Eng.*, Santiago, Chile, 2017, Paper 3902.
[25] V. Silva et al., "Exploring risk-targeted hazard maps for Europe," *Earthquake Spectra*, vol. 32, no. 2, pp. 1165–1186, 2016, doi: 10.1193/112514eqs198m.
[26] Tata cara perencanaan ketahanan gempa untuk struktur bangunan gedung dan non gedung, SNI 1726:2019, 2019. [Online]. Available: https://sitaba.pu.go.id/publikasi/6977fb4f-d02f-4fd0-a857-65219c38f24e
[27] Badan Nasional Penanggulangan Bencana, "Peraturan Kepala BNPB Nomor 02 Tahun 2012 tentang Pedoman Umum Pengkajian Risiko Bencana," BNPB, Jakarta, Indonesia, 2012. [Online]. Available: https://bpba.acehprov.go.id/media/2022.09/perka_951.pdf
[28] A. Soehaimi et al., "Seismotectonic and probabilistic seismic hazard of Sunda Strait region," *EGUsphere*, 2023, doi: 10.5194/egusphere-2023-423.
[29] S. Widiyantoro et al., "Implications for megathrust earthquakes and tsunamis from seismic gaps south of Java Indonesia," *Sci. Rep.*, vol. 10, p. 15274, 2020, doi: 10.1038/s41598-020-72142-z.
[30] P. Supendi et al., "On the potential for megathrust earthquakes and tsunamis off the southern coast of West Java and southeast Sumatra, Indonesia," *Nat. Hazards*, vol. 116, pp. 1315–1328, 2023, doi: 10.1007/s11069-022-05696-y.
[31] Kementerian Pekerjaan Umum dan Perumahan Rakyat. (2025). Peran PuSGeN dalam Tata Kelola Keselamatan dan Keamanan Infrastruktur Bangunan Tahan Gempa [Online]. Pusat Studi Gempa Nasional (PuSGeN).
[32] Y. Bozorgnia and V. V. Bertero, Eds., *Earthquake Engineering*. Boca Raton, FL: CRC Press, 2004, doi: 10.1201/9780203486245.